GEOPHYSICS, VOL. 83, NO. 2 (MARCH-APRIL 2018); P. P1–P8, 7 FIGS.
10.1190/GEO2017-0327.1

Check for updates

Downloaded 01/05/18 to 138.67.12.184. Redistribution subject to SEG license or copyright; see Terms of Use at http://library.seg.org/

Multicomponent distributed acoustic sensing: Concept and theory

Ivan Lim Chen Ning[1] and Paul Sava[1]

ABSTRACT

Distributed acoustic sensing (DAS) data are increasingly used in geophysics. Lower in cost and higher in spatial resolution, DAS data are appealing, especially in boreholes in which optical fibers are readily available. DAS has the potential to become a permanent reservoir monitoring tool with a reduced sensing time interval. To accomplish this goal, it is critical that DAS can record all wave modes to fully characterize reservoir properties. This goal can be achieved by recording the complete strain tensor consisting of 6C. Conventional DAS provides projections of these components along the optical fiber by observing deformation along the fiber. To obtain the entire 6C strain tensor, we have developed an approach using multiple strain projections measured along optical fibers with judiciously chosen geometry specifically. We evaluate designs combining multiple helical configurations or a single helical configuration together with a straight optical fiber that allow access to multiple strain projections. We group multiple strain projections in a given spatial window to perform reconstruction of the entire strain tensor in a least-squares sense under the assumption that the seismic wavelength is larger than the analysis window size. We determine how optimal optical fiber parameters can be selected using a scan of the entire configuration space and analyzing the condition number associated with the geometry of the optical fibers. We develop our method through synthetic experiments using realistic fiber geometry and wavefields of arbitrary complexity.

INTRODUCTION

Distributed acoustic sensing (DAS) is rapidly gaining popularity in the oil and gas industry, especially for vertical seismic profile imaging and reservoir monitoring (Mestayer et al., 2011; Cox et al., 2012; Mateeva et al., 2012, 2013; Daley et al., 2013; Madsen et al., 2013). The advantages of DAS for borehole applications in terms of cost, the deployment mechanism, and spatial resolution make its use more attractive than conventional geophone acquisition (Lumens et al., 2013; Mateeva et al., 2013). The application of optical fiber in wells is not an unfamiliar method because optical fiber has long been used for temperature measurement known as distributed temperature sensing (Karaman et al., 1996; Hartog, 2000).

DAS transforms an optical fiber into a distributed array of strain measuring tools. The acquisition requires an interrogator unit (IU) to send laser pulses into the optical fiber and detect back-scattered light from inhomogeneities along the fiber. These inhomogeneities are impurities caused either deliberately during manufacturing with the use of dopants or by manufacturing defects (Uzunoglu, 1981; Tsujikawa et al., 2005). The backscattering generated by these inhomogeneities is called Rayleigh scattering. Analyzing the changes in phase of the back-scattered light gives access to information such as strain as a function of distance from the IU through coherent optical time-domain reflectometry (COTDR).

The underlying principle behind COTDR is to analyze the phase difference between the back-scattered signal from two points along an optical fiber (Bakku, 2015). The distance separating the two points is known as the gauge length. Introducing disturbance to the optical fiber generates perturbation to the otherwise constant phase difference between the two measurement points. This additional phase difference is quasi-linearly proportional to the average axial strain between the two points. Legacy DAS systems that analyze backscatters require a gauge length of approximately 1 m to achieve acceptable signal-to-noise ratio (S/N) measurements. However, recent hardware uses specially designed optical fibers and the gauge length can be reduced to 0.05 m while maintaining an acceptable S/N (Farhadiroushan et al., 2016). In this paper, we focus on a range of gauge lengths and emphasize smaller sizes that characterize the

Manuscript received by the Editor 20 May 2017; revised manuscript received 12 October 2017; published ahead of production 08 November 2017; published online 05 January 2018.
[1]Colorado School of Mines, Center for Wave Phenomena, Department of Geophysics, Golden, Colorado, USA. E-mail: ivanlimchenning@mines.edu; psava@mines.edu.
© 2018 Society of Exploration Geophysicists. All rights reserved.

Downloaded 01/05/18 to 138.67.12.184. Redistribution subject to SEG license or copyright; see Terms of Use at http://library.seg.org/

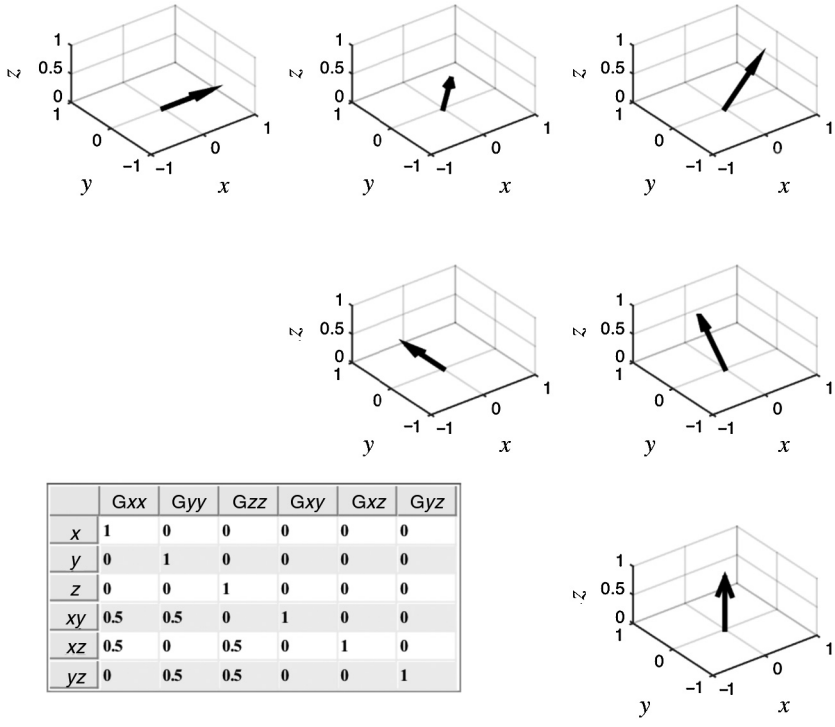
instrumentation currently being deployed or that is expected to come online shortly.

As indicated by Lumens (2014) and Bakku (2015), the DAS system is more sensitive in the axial direction compared with the radial direction, thus reducing the DAS measurable data to the axial strain, which can be measured with an acceptable S/N. Most of the DAS deployments are focused on borehole applications and multicomponent seismic data are desirable for use in seismic characterization and monitoring (Davis et al., 2003; Stewart et al., 2003). Several publications suggest that 3C sensing using DAS is possible (den Boer et al., 2012, 2013; Crickmore and Hill, 2014; Hartog et al., 2014; Kragh et al., 2014; Farhadiroushan et al., 2015); however, no published work details mechanisms for extracting the 6C strain tensor from axial strain measurement using DAS. Geophones can record multicomponent data; however, they are costly and do not provide the dense spatial sampling of DAS. In this paper, we investigate possibilities for using different optical fiber configurations to gain access to multicomponent information.

We propose an approach for acquiring multicomponent data with the use of multiple strain projection measurements. To achieve these measurements, we use various helical fiber configurations. Existing helical optical fiber configurations for DAS (den Boer et al., 2013; Kuvshinov, 2016; Hornman, 2017) are designed to detect broadside acoustic signals, i.e., waves that arrive at large angles relative to the axis of the optical fiber. However, here we are interested in using the projections of the strain tensor along the optical fiber to reconstruct the full 6D strain tensor at points along the optical fiber. Using the characteristics of the helix and the axial strain measurement of the optical fiber, we can evaluate the entire strain tensor at every measuring location under the assumption that the seismic wavelength is significantly longer than the helix period. We show the theoretical relationship between the measured axial strain in the optical fiber and the full strain tensor in the surrounding area, and we demonstrate the applicability of this strategy using 3D synthetic examples of complex seismic wavefields. Our method accounts for the gauge length characterizing the DAS measurements.

In this paper, we assume a DAS system that can acquire data using gauge lengths of 0.2 and 1.0 m with realistic lengths of optical fiber cable. The gauge length of 1.0 m has been reported in the literature by Daley et al. (2013). Using this gauge length, we consider a cable that can typically be deployed for reservoir monitoring in a borehole environment; a helically wound cable (Kuvshinov, 2016; Hornman, 2017) increases the overall length of the optical fiber. If we assume the seismic bandwidth of 10–100 Hz, the current DAS systems can provide a dynamic range 80 dB or higher. If we deploy an optical fiber cable with improved reflective properties as suggested by Farhadiroushan et al. (2016), we may further increase the dynamic range. Thus, we assume a system comparable with currently available acquisition systems, which might improve in the future. The other gauge length we consider is 0.2 m, which would be beneficial for engineering applications using shorter cables, and it is capable of acquiring higher frequencies.

We begin by reviewing the theoretical aspects of the proposed approach, followed by 3D synthetic examples. While discussing the results, we also review the associated assumptions and limitations to this approach. We then propose a feasible configuration that allows our method to be practically implemented using current optical fiber technology.



	Gxx	Gyy	Gzz	Gxy	Gxz	Gyz
x	1	0	0	0	0	0
y	0	1	0	0	0	0
z	0	0	1	0	0	0
xy	0.5	0.5	0	1	0	0
xz	0.5	0	0.5	0	1	0
yz	0	0.5	0.5	0	0	1

Figure 1. Examples of strain tensor projection onto the vectors pointing along and oblique relative to the directions of the x-, y-, and z-axes. The columns of the bottom left table show the contribution of strain elements in terms of the **G** matrix in equation 2, and the rows represent the different vectors, respectively.

THEORY

The axial strain measurement by DAS is a projection of the strain tensor from the surrounding area as a function of the optical fiber position. We use the intrinsic coordinate system of a curve as the local coordinate system for the optical fiber with respect to the global coordinate system (Lin and Pisano, 1988). Because DAS measures axial strain, it suffices to use the tangent vector along the optical fiber to perform strain tensor projection. We exploit the helical geometry as a tool to measure different projections of the strain field onto the optical fiber; i.e., we measure the projection of the surrounding strain tensor along the optical fiber as a function of the pitch angle and azimuth angles. We adopt the definition of Lin and Pisano (1988) on pitch angle as the complement of the angle between the tangent vector and the axial direction of the DAS cable.

The relationship between the axial strain measured by the optical fiber and the strain tensor of the surrounding area can be expressed through the strain tensor coordinate transformation relationship as (Young and Budynas, 2002)

$$\bar{\boldsymbol{\varepsilon}} = \mathbf{R}\boldsymbol{\varepsilon}\mathbf{R}^{\mathbf{T}}, \tag{1}$$

where $\bar{\boldsymbol{\varepsilon}}$ and $\mathbf{R}$ denote the transformed strain tensor and the transformation (also known as rotation) matrix, respectively. We rearrange equation 1 as

$$\mathbf{b} = \mathbf{G}\mathbf{m}, \tag{2}$$

where $\mathbf{b}$ and $\mathbf{m}$ are the vectorized transformed and original strain tensors, respectively. Matrix $\mathbf{G}$ is the expansion of equation 1 using the transformation matrix $\mathbf{R}$. The axial strain measurement reduces $\mathbf{b}$ and $\mathbf{G}$ to single-row matrices. Figure 1 illustrates the strain tensor projections onto a vector together with the $\mathbf{G}$ matrix representation.

In equation 2, the projection $\mathbf{b}$ refers to a point along the optical fiber. Because DAS measures an average strain within a gauge length, we introduce an averaging operator $\mathbf{A}$ to account for this effect. The gauge length averaging is as follows:

$$\overset{\mathbf{d}}{\begin{bmatrix} d_1 \\ \vdots \\ d_M \end{bmatrix}} = \frac{1}{L} \overset{\mathbf{A}}{\begin{bmatrix} \Delta S & \Delta S & 0 & 0 & 0 \\ 0 & 0 & \ddots & 0 & 0 \\ 0 & 0 & 0 & \Delta S & \Delta S \end{bmatrix}} \overset{\mathbf{b}}{\begin{bmatrix} b_1 \\ \vdots \\ b_N \end{bmatrix}}, \tag{3}$$

where N and M are the number of measurements before and after performing gauge length averaging, respectively. The function ΔS is the spacing between the strain measurements and L denotes the gauge length. To perform strain tensor reconstruction, we group consecutive strain measurements along the optical fiber within a defined window. These measurements represent the data vector $\mathbf{d}$ and account for strain averaging within a gauge length. The reconstructed strain tensor refers to the middle of the window. Here, we make the assumption that the seismic wavelength is much greater than the length of the window. This assumption is important so that we can group multiple measurements within the window to refer to the same strain tensor field at a given location. A large seismic wavelength relative to the considered window along the fiber provides a slowly varying strain tensor field, which we can assume to be invariant within the window used for its reconstruction.

We can solve for the strain components (the model $\mathbf{m}$ in equation 2) in a least-squares sense, based on the known kernel or forward operator $\mathbf{G}$ and averaging operator $\mathbf{A}$. The data $\mathbf{d}$ are consecutive axial strain measurements along the helical optical fiber within a window as indicated earlier (this implies that the strain tensor that we are reconstructing does not change within this window

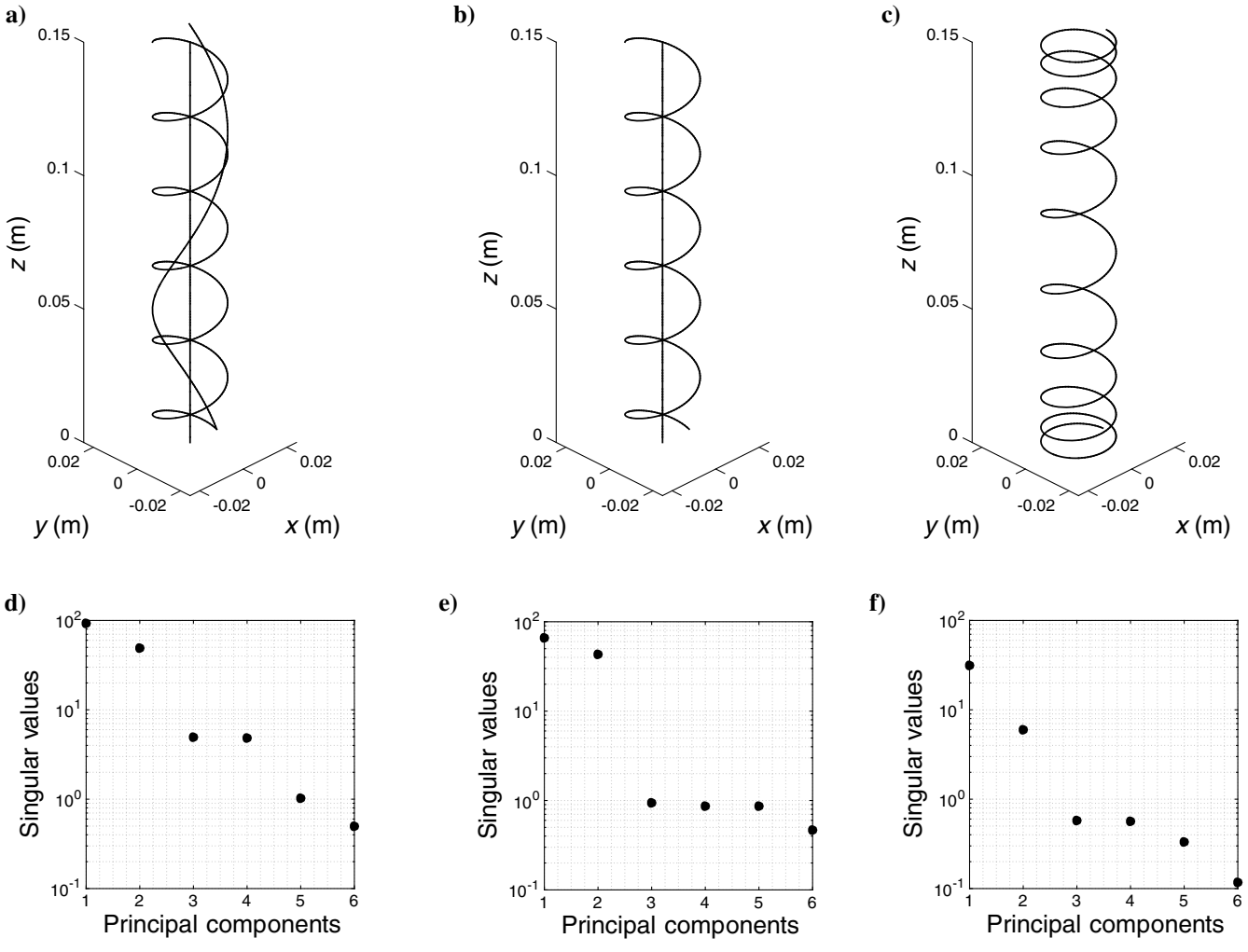


Figure 2. Examples of optical fiber configurations with (a) two helical optical fibers with pitch angles of 20° and 60° and a single straight optical fiber and (b) one helical optical fiber with a pitch angle of 20° and a single straight optical fiber. (c) A simplified example of the chirping helix configuration for plotting purposes. The helixes are constructed with a diameter of 0.0244 m (approximately 1 in). (d-f) SVD of the Gram matrix in equation 5 for the corresponding configurations. The Gram matrix uses measurements in a window of 5 m.

Downloaded 01/05/18 to 138.67.12.184. Redistribution subject to SEG license or copyright; see Terms of Use at http://library.seg.org/

Downloaded 01/05/18 to 138.67.12.184. Redistribution subject to SEG license or copyright; see Terms of Use at http://library.seg.org/

or segment along the optical fiber), and the model $\mathbf{m}$ is the strain tensor at a given location. We reiterate that the measurements contained in vector $\mathbf{d}$ are subject to averaging within a gauge length; this effect is captured by the averaging matrix $\mathbf{A}$ of known size. We minimize the objective function:

$$\mathcal{J} = \frac{1}{2}\|\mathbf{W}(\mathbf{AGm} - \mathbf{d})\|^2, \tag{4}$$

where $\mathbf{W}$ is a weighting operator that represents the uncertainty of the projection matrix derived from the geometry of the optical fiber. For simplicity, the reconstructions in the following examples, we use identity as the weighting matrix. The model $\mathbf{m}$ can be expressed as

$$\mathbf{m} = (\mathbf{G^T A^T A G})^{-1}\mathbf{G^T A^T d}. \tag{5}$$

To investigate the types of configurations that allow us to perform strain tensor reconstruction, we explore the configuration by den Boer et al. (2013) that uses two helical optical fiber and a single straight optical fiber in the middle. The total of three optical fibers, in principle, could provide 3C sensing. However, our target reconstruction is a 6C strain tensor. To analyze the suitability of this three-optical-fiber configuration, we use two helical optical fibers with a diameter of 0.0244 m (approximately 1 in) together with the pitch angles of 20° and 60°, respectively. Because DAS with a small gauge length is achievable (Farhadiroushan et al., 2016), we use a gauge length of 0.1 m. To accurately analyze the DAS acquisition that measures average strain within a gauge length, we use the averaging matrix $\mathbf{A}$ together with the projection matrix $\mathbf{G}$. Using these matrices, we calculate the singular-value decomposition (SVD) of the Gram matrix $\mathbf{G^T A^T A G}$. The singular values from the SVD analysis of the Gram matrix provide insight into the suitability of a given configuration for strain tensor reconstruction using our approach. An example of this three-optical-fiber configuration is illustrated in Figure 2a together with the singular values after performing SVD in Figure 2d. In the SVD analysis, the Gram matrix uses measurements in a window of 5 m, assuming that the seismic wavelength is much greater than the window. Based on the SVD results, the singular values of the Gram matrix indicate that it is full rank and can be used for strain tensor reconstruction.

We further simplify the three-optical-fiber configuration by omitting the helical optical fiber with the pitch angle of 60°. This gives us a configuration using only two optical fibers. An example of this configuration is shown in Figure 2b, and the corresponding singular values from SVD are shown in Figure 2e. Although there is some slight reduction in the singular values, this simplified configuration is still full rank and can be used for strain tensor reconstruction. In this paper, we show numerical examples using this simplified configuration of two optical fibers.

We also investigate a different configuration by introducing a varying pitch angle helical optical fiber (we refer to this configuration as a chirping helical optical fiber). An example of such a configuration is shown in Figure 2c with a diameter of 0.0244 m (approximately 1 in), where we perform a pitch angle down-sweep and up-sweep within a window of 0.15 m, giving a total of 10 complete helix turns. The example configuration is not used for the SVD analysis because this is for plotting purposes only. The configuration we use that gives the singular values in Figure 2f is a pitch angle down-sweep and up-sweep within a window of 5 m giving a total of 100 number of turns. We emphasize that we assume the seismic wavelength is much greater than the window. The singular values are slightly lower than that of the previous configurations, but the chirping helix configuration is still full rank. A full-rank Gram matrix indicates that we are able to reconstruct the strain tensor. It is worth noting that the chirping configuration only requires one optical fiber, albeit with increased complexity that may be difficult to engineer using an optical fiber and may increase the complexity of deployment.

Furthermore, we examine the effects of the helical optical fiber design parameters on the Gram matrix by performing a parameter scan as shown in Figure 3. We fix the diameter of the helical optical fiber at 0.0244 m (approximately 1 in) to restrict the parameter search space. For the dual-optical-fiber configuration, we find the optimum design parameters (i.e., the window length for reconstruction and the pitch angle of the helical optical fibers) associated with low condition numbers, as shown in Figure 3a and 3b for gauge lengths of 0.2 and 1.0 m, respectively. If a given reconstruction window captures sufficient strain projections that can fully characterize the surrounding strain tensor, further increasing the reconstruction window size

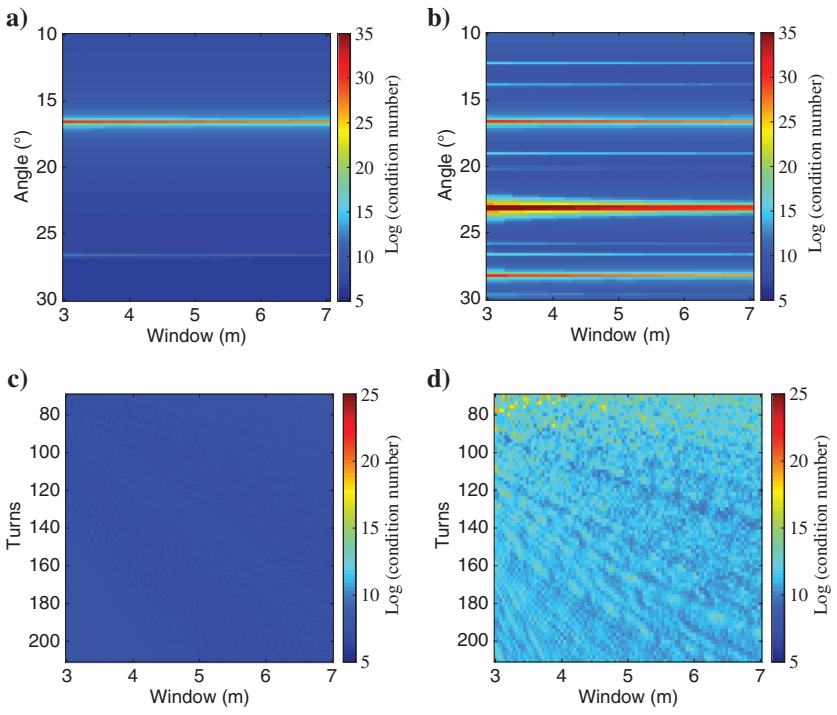


Figure 3. Condition number of the Gram matrix using a fixed diameter at 0.0244 m (approximately 1 in) with the dual-optical-fiber configuration at gauge lengths of (a) 0.2 m and (b) 1.0 m for window from 3 to 7 m and pitch angle from 10° to 30°. Similarly, the condition number with the chirping helical optical fiber configuration at gauge lengths of (c) 0.2 m and (d) 1.0 m for a window from 3 to 7 m and the number of turns within a window from 10 to 210 turns.

Downloaded 01/05/18 to 138.67.12.184. Redistribution subject to SEG license or copyright; see Terms of Use at http://library.seg.org/

does not improve the condition number because it has already reached an optimum value, as shown in Figure 3a and 3b. Nevertheless, the reconstruction window should be kept at a minimum to preserve the spatial resolution. Similarly, using the chirping helical optical fiber configuration, we scan for the optimum design parameters (i.e., window length for reconstruction and the number of helical turns within a window) associated with low condition numbers, as shown in Figure 3c and 3d for gauge lengths of 0.2 and 1.0 m, respectively.

The strain measurement by the DAS system using a helical geometry undergoes strain averaging in the azimuthal direction along the optical fiber within a gauge length. When the gauge length is equal to a multiple of the helix lead (the axial advance of a helix for a complete 360° turn), the DAS measurement does not contain azimuthal information, which translates into a high condition number. Using the dual-optical-fiber configuration with a cable diameter of 0.0244 m (approximately 1 in) and a gauge length of 0.2 m, as shown in Figure 3a, we observe a large condition number linear feature for pitch angles between 16° and 17°. Because every single measurement within this pitch angle range contains little or no azimuthal information, the condition number remains high regardless of the window size. Increasing the gauge length to 1.0 m in Figure 3b, we observe an increasing number of high condition number features. This increase in number is due to the higher azimuthal averaging along the helical fiber within a longer gauge length. However, the range for the condition number of both gauge lengths remains relatively consistent, suggesting that accurate reconstruction can be achieved with careful selection of design parameters.

In the case of a chirping helical optical fiber configuration with a gauge length of 0.2 m in Figure 3c, we can see that the condition number range is significantly lower than the dual optical fibers of the same gauge length. The chirping helix provides a larger range of strain projections, which improves the reconstruction results as demonstrated by the overall low condition numbers. However, the condition number range increases rapidly with a larger gauge length of 1.0 m, as shown in Figure 3d. The condition number amplified more than 10 times suggests that the chirping helix configuration can only be deployed if a small gauge length is used.

Numerical examples

Using synthetic examples of complex seismic wavefields, we illustrate the reconstruction of the 6D strain tensor from axial strain measurements along the proposed optical fiber geometries. In the reconstruction, we choose a window size of 5 m that is approximately six times smaller than the smallest seismic wavelength of 33.33 m. The following examples are simulated using elastic finite-difference modeling with a velocity model containing a low-velocity Gaussian anomaly to produce wavefield triplications as shown in Figure 4c. A snapshot of the wavefield triplication is shown in the bottom right panel of Figure 4d. We use a gauge length and a channel spacing of 0.2 m for our DAS data simulation. The channel spacing refers to the distance between consecutive average strain measurements within a gauge length. Although such a small gauge length is possible, as indicated by Farhadiroushan et al. (2016), we also perform simulations using a gauge length and channel spacing used in more conventional DAS acquisition systems at 1.0 m. Using such short gauge lengths, the effect of wavenumber filtering discussed by Dean et al. (2017) is negligible. In our setup, we assume perfect coupling between the optical fiber to the surroundings (i.e., cementing), which is a common assumption for DAS analysis of any geometry.

Figure 4a shows the experiment setup in which the dot represents the source location and the straight line with the coordinates (x_b, y_b) is a borehole segment in which the helical configurations are positioned. Figure 4b shows the observed strain tensor along the straight line at (x_b, y_b) in a strain tensor matrix layout, which is the target for strain reconstruction. The horizontal axis of the individual panels represents the reconstructed measurements along the optical fiber, and the vertical axis represents time. Figure 5a shows the reconstructed strain tensor using the dual-optical-fiber configuration with a helical optical fiber and a straight optical fiber in the middle using a gauge length and channel spacing of 0.2 m. The helical optical fiber has a diameter of 0.0244 m (approximately 1 in) and a pitch angle of 20°. Using this configuration, we are able to successfully reconstruct the strain tensor that is evident on the difference plot

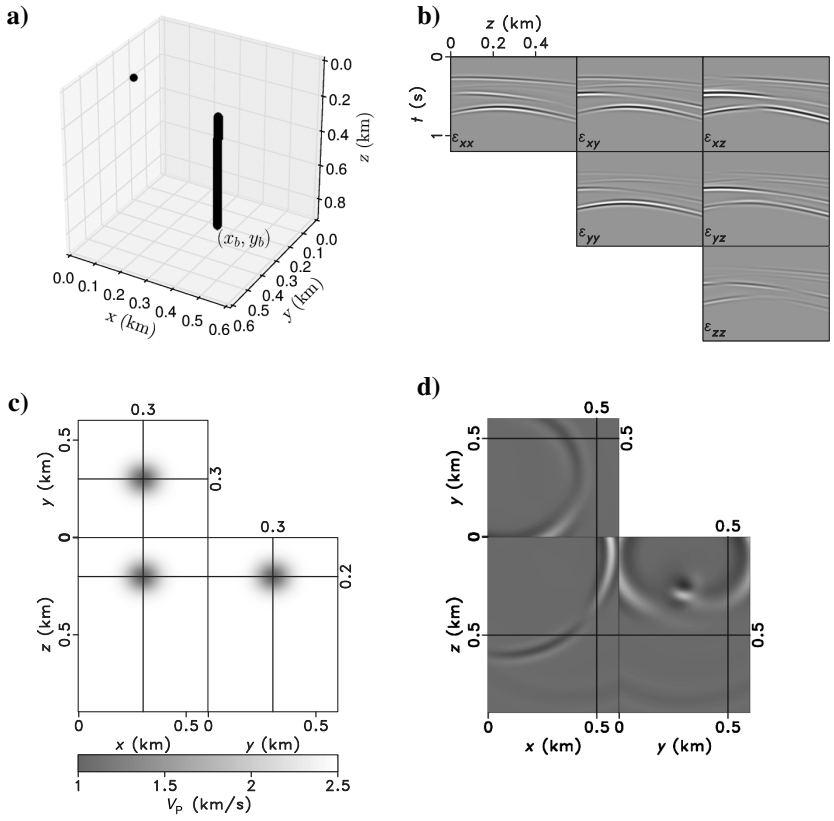


Figure 4. (a) Schematic representation of a DAS experiment depicting the source (dot) and receiver (line) locations. (b) The ideal strain tensor that we would like to reconstruct from DAS measurements. (c) The P-wave velocity model containing a low-velocity Gaussian anomaly designed to produce wavefield triplications. The S-wave velocity is half of the P-wave velocity. (d) A snapshot of the vertical displacement wavefield.

Downloaded 01/05/18 to 138.67.12.184. Redistribution subject to SEG license or copyright; see Terms of Use at http://library.seg.org/

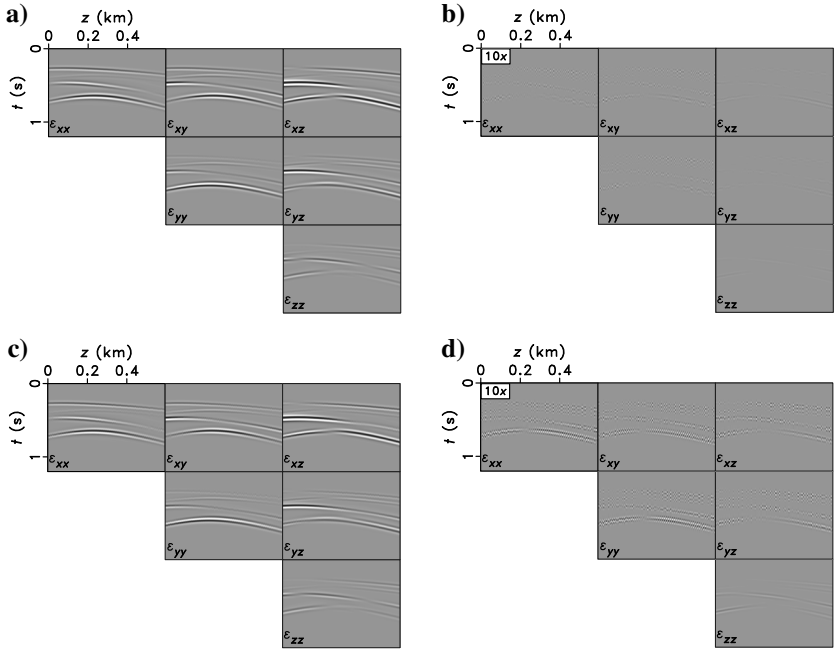


Figure 5. Strain tensor reconstructed using the dual-optical-fiber configuration with one helical and one straight optical fiber shown in Figure 2b using a gauge length and channel spacing of (a) 0.2 m and (c) 1.0 m. (b and d) The difference between the ideal strain tensor in Figure 4b and the respective reconstructed tensor in (a and c) magnified 10 times.

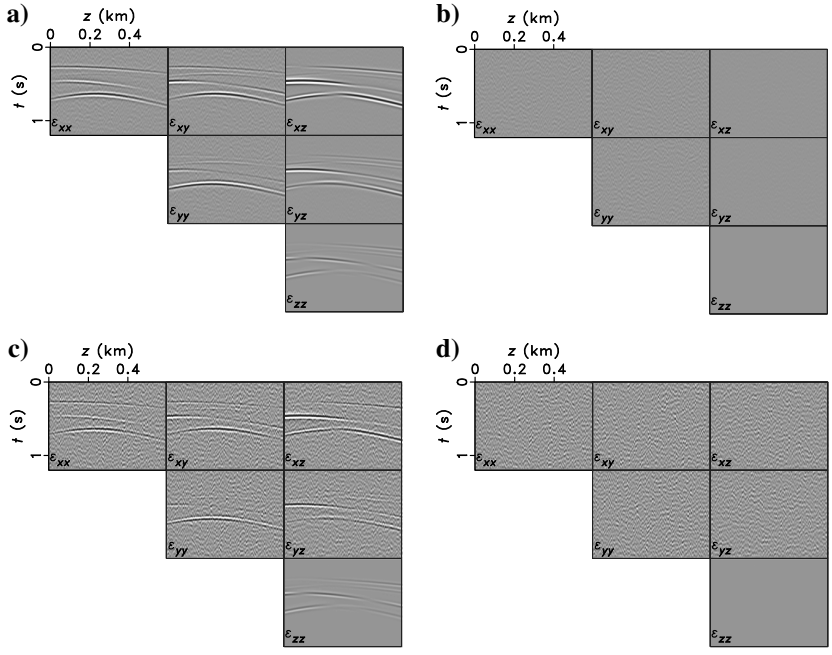


Figure 6. Strain tensor reconstructed using the chirping helical optical fiber configuration using a gauge length and channel spacing of 0.2 m is shown in (a), and (c) shows the reconstruction under the influence of random noise with 5% of the maximum data amplitude and band-limited to the data band. The difference between the ideal strain tensor in Figure 4b and the respective reconstructed tensor in (a and c) is shown in (b) magnified 10 times and (d).

between the observed and reconstructed strain tensor amplified 10 times, as shown in Figure 5b. We quantify the quality of strain reconstruction using

$$\eta = \frac{\|\mathbf{m}^{\text{obs}} - \mathbf{m}^{\text{rec}}\|^2}{\|\mathbf{m}^{\text{obs}}\|^2} 100, \qquad (6)$$

where $\mathbf{m}^{\text{obs}}$ represents the observed strain tensor and $\mathbf{m}^{\text{rec}}$ represents the reconstructed strain tensor. The scalar values for η in the case of the dual-optical-fiber configuration are less than 0.4%. Figure 5c shows the reconstructed strain tensor using the same configuration but with the gauge length and channel spacing at 1.0 m. The differences shown in Figure 5d (also amplified 10 times) suggest that the increase of gauge length has a negative impact on our reconstruction. Although the calculated values for η increase overall with the larger gauge length, the highest η is less than 4.5%, which is a perfectly acceptable accuracy level for practical applications.

We perform the same numerical analysis on the chirping helical optical fiber configuration with a diameter of 0.0244 m (approximately 1 in), where we perform a pitch angle down-sweep and up-sweep within a window of 5 m, giving a total of 100 number of turns. Figure 6a shows the reconstructed strain tensor with a gauge length and channel spacing of 0.2 m. The results show that we are able to achieve a comparable reconstruction quality to the dual-optical-fiber configuration by observing the amplified 10 times difference plot in Figure 6b. The η values for the chirping configuration are less than 0.3%. The reconstruction results using a gauge length of 1.0 m are not shown here due to the significant uncertainty associated with the massive condition number, as shown in Figure 3d.

We also test the reconstruction process for both configurations by adding random noise with 5% of the maximum amplitude of the data and in the data frequency band. Therefore, in places where the signals are weak, the noise overwhelms the signal. Using the dual-optical-fiber configuration with gauge length and channel spacing of 0.2 m, Figure 7a shows that we are able to reconstruct the strain tensor. The difference plot in Figure 7b shows primarily random noise. The strain tensor reconstruction with a larger gauge length and channel spacing at 1.0 m is shown in Figure 7c. Although the reconstructed strain tensor is contaminated with noise, we can observe some of the stronger arrivals in all of the strain components. The difference plot shown in Figure 7d contains primarily noise.

We use the same noise characteristics for the chirping configuration. Figure 6c shows the reconstructed strain tensor using the chirping

Downloaded 01/05/18 to 138.67.12.184. Redistribution subject to SEG license or copyright; see Terms of Use at http://library.seg.org/

configuration with a gauge length and channel spacing of 0.2 m with added noise. We successfully reconstruct the strain tensor, although it contains slightly higher noise level than the dual-optical-fiber configuration. The difference plot in Figure 6d contains primarily noise. The reconstruction using a larger gauge length and channel spacing at 1.0 m is not shown here because the noise overwhelms the actual data due to the large condition number associated with this configuration.

DISCUSSION

Our investigation shows that the full strain tensor can be reconstructed with a high level of accuracy either using two optical fibers (one helical optical fiber with a pitch angle of 20° and a straight optical fiber) or a single chirping helical optical fiber. However, a relatively small, but achievable, gauge length is required to ensure good (low η) reconstruction under the influence of noise for small-diameter helical configurations. This is often restricted by the dimension of the borehole. If we consider applications such as surface seismic acquisition in which the dimensions are more relaxed, increasing the diameter of the helical configuration allows for a larger gauge length, which in turn enables strain tensor reconstruction in noisier environments.

As shown in the earlier sections, we can reconstruct the strain tensor using only a single chirping helical optical fiber. However, we also show that the reconstruction under the influence of noise is inferior to the two-optical-fiber configuration. Although we only need to deploy a single optical fiber, this comes at the expense of reconstruction quality. In addition, the engineering and deployment of such a complex configuration are challenging. An alternative is to use two optical fibers with one helical optical fiber and one straight optical fiber. Besides being more robust in the presence of noise, the engineering and deployment are less challenging than the chirping helical optical fiber.

Overall, the dual-optical-fiber configuration has a lower condition number for the Gram matrix compared with the single chirping helical optical fiber. The condition number gives us a measure of how sensitive our reconstruction is under the presence of noise. A small condition number implies that we are able to reconstruct the strain tensor well under the influence of noise. In our examples, using a gauge length of 0.2 m allows us to reconstruct a good quality (low η) strain tensor for both configurations. However, increasing the gauge length to 1.0 m increases the condition number, which is evident from the increased level of noise after reconstruction and especially in the chirping configuration in which the results are overwhelmed by noise. However, the dual-optical-fiber configuration can be deployed with currently available DAS systems.

All the design parameters for the helical optical fiber affect one another, and there is no one optimum set of parameters that may suit all situations. However, we may define some limiting parameters, such as the diameter of the helix (in the case of a borehole), and then adjust the remaining parameters based on the noise and accuracy requirements. In the end, the design goal is to obtain configuration(s) that have a full-rank Gram matrix $\mathbf{G^T A^T A G}$ calculated from the averaging $\mathbf{A}$ and projection matrix $\mathbf{G}$. Such design parameter estimation is shown in Figure 3 by evaluating the condition numbers for different geometries. The weighting operator shown in equation 4 can be used to reduce the reconstruction errors due to the uncertainty of the optical fiber geometry, which translates into the uncertainty of the projection matrix $\mathbf{G}$. The shape-sensing method of Moore and Rogge (2012) is one mechanism to detect the actual shape of the deployed fibers, thus reducing the uncertainty in the geometry of the optical fiber.

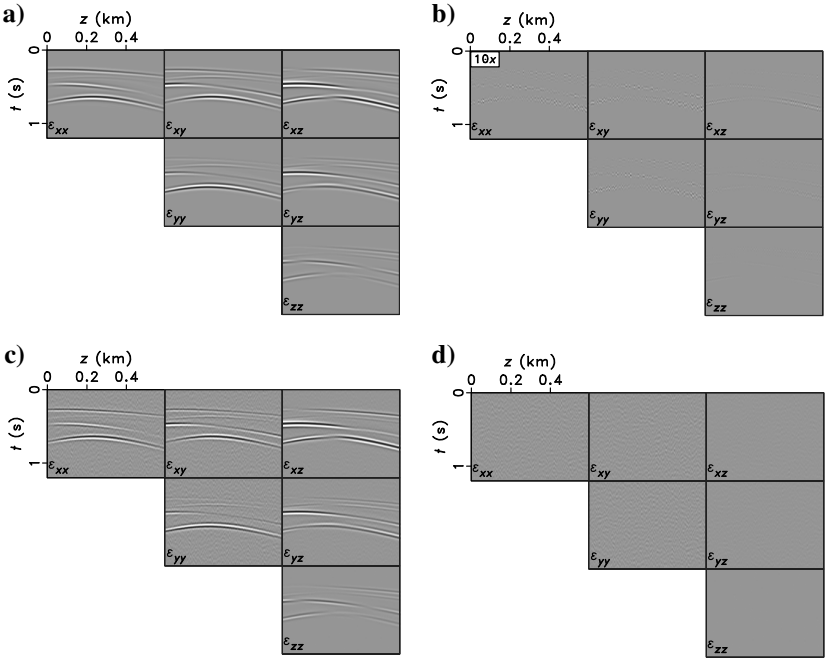


Figure 7. Strain tensor reconstructed from data containing random noise with 5% of the maximum data amplitude and band-limited to the data band using the dual-optical-fiber configuration with one helical optical fiber and one straight optical fiber shown in Figure 2b using a gauge length and channel spacing of (a) 0.2 m and (c) 1.0 m. (b and d) The difference between the ideal strain tensor in Figure 4b and the respective reconstructed tensor in (a and c).

CONCLUSION

We demonstrate that multicomponent DAS is achievable using strain projection measured along optical fibers to reconstruct all components of the strain tensor. Several optical fiber configurations can be used to accomplish multiple strain projection measurements. The chirping helical optical fiber can reconstruct the strain tensor, but the manufacturing and deployment of such a configuration may prove to be challenging. A more practical configuration uses a helical optical fiber and a straight optical fiber, which is more robust in the presence of noise. Because DAS is a rapidly evolving technology, DAS with a smaller gauge length is imminent. Using conventional and smaller gauge lengths, we are able to accurately reconstruct the entire strain tensor, especially when the diameter of the helical optical fiber is small, as in the case of a borehole environment. Our numerical examples indicate that this type of acquisition can be used to reconstruct the full strain tensor for wavefields of arbitrary complexity and in the presence of noise in the band of the seismic data.

ACKNOWLEDGMENTS

We would like to thank the sponsors of the Center for Wave Phenomena, whose support made this research possible and M. Karrenbach of OptaSense for fruitful discussions. We are grateful to associate editor G. Drijkoningen and the anonymous reviewers for their valuable comments that helped to improve the manuscript. The reproducible numeric examples in this paper use the Madagascar open-source software package (Fomel et al., 2013) freely available from http://www.ahay.org.

REFERENCES

Bakku, S. K., 2015, Fracture characterization from seismic measurements in a borehole: Ph.D. thesis, Massachusetts Institute of Technology.

Cox, B., P. Wills, D. Kiyashchenko, J. Mestayer, J. Lopez, S. Bourne, R. Lupton, G. Solano, N. Henderson, D. Hill, and J. Roy, 2012, Distributed acoustic sensing for geophysical measurement, monitoring and verification: CSEG Recorder, **37**, 7–13.

Crickmore, R., and D. Hill, 2014, Fibre optic cable for acoustic/seismic sensing: WO Patent App. PCT/GB2013/052, 795.

Daley, T. M., B. M. Freifeld, J. Ajo-Franklin, S. Dou, R. Pevzner, V. Shulakova, S. Kashikar, D. E. Miller, J. Goetz, J. Henninges, and S. Lueth, 2013, Field testing of fiber-optic distributed acoustic sensing (DAS) for subsurface seismic monitoring: The Leading Edge, **32**, 699–706, doi: 10.1190/tle32060699.1.

Davis, T. L., M. J. Terrell, R. D. Benson, R. Cardona, R. R. Kendall, and R. Winarsky, 2003, Multicomponent seismic characterization and monitoring of the CO_2 flood at Weyburn Field, Saskatchewan: The Leading Edge, **22**, 696–697, doi: 10.1190/1.1599699.

Dean, T., T. Cuny, and A. H. Hartog, 2017, The effect of gauge length on axially incident p-waves measured using fibre optic distributed vibration sensing: Geophysical Prospecting, **65**, 184–193, doi: 10.1111/1365-2478.12419.

den Boer, J., J. Koelman, J. Pearce, A. Franzen, P. Lumens, and D. Joinson, 2012, Fiber optic cable with increased directional sensitivity: WO Patent App. PCT/US2012/042, 919.

den Boer, J., A. Mateeva, J. Pearce, J. Mestayer, W. Birch, J. Lopez, K. Hornman, and B. Kuvshi, 2013, Detecting broadside acoustic signals with a fiber optical Distributed Acoustic Sensing (DAS) assembly: WO Patent App. PCT/US2012/069, 464.

Farhadiroushan, M., D. Finfer, D. Strusevich, S. Shatalin, and T. Parker, 2015, Non-isotropic acoustic cable: WO Patent App. PCT/GB2014/052, 679.

Farhadiroushan, M., T. Parker, and S. Shatalin, 2016, Method and apparatus for optical sensing: WO Patent App. PCT/GB2016/050, 625.

Fomel, S., P. Sava, I. Vlad, Y. Liu, and V. Bashkardin, 2013, Madagascar: Open-source software project for multidimensional data analysis and reproducible computational experiments: Journal of Open Research Software, **1**, e8, doi: 10.5334/jors.ag.

Hartog, A., 2000, Distributed fiber-optic sensors: Principles and applications, *in* K. T. V. Grattan, and B. T. Meggitt, eds., Optical fiber sensor technology: Springer, 241–301.

Hartog, A., J. Martin, D. Donno, and B. Papp, 2014, Fiber optic distributed vibration sensing with directional sensitivity: WO Patent App. PCT/US2014/042, 226.

Hornman, J., 2017, Field trial of seismic recording using distributed acoustic sensing with broadside sensitive fibre-optic cables: Geophysical Prospecting, **65**, 35–46, doi: 10.1111/1365-2478.12358.

Karaman, O. S., R. L. Kutlik, and E. L. Kluth, 1996, A field trial to test fiber optic sensors for downhole temperature and pressure measurements, West Coalinga Field, California: Presented at the SPE Western Regional Meeting, Society of Petroleum Engineers, SPE 35685.

Kragh, E., E. Muyzert, J. Robertsson, D. Miller, and A. Hartog, 2014, Seismic acquisition system including a distributed sensor having an optical fiber: US Patent 8, 924, 158.

Kuvshinov, B., 2016, Interaction of helically wound fibre-optic cables with plane seismic waves: Geophysical Prospecting, **64**, 671–688, doi: 10.1111/1365-2478.12303.

Lin, Y., and A. P. Pisano, 1988, The differential geometry of the general helix as applied to mechanical springs: Journal of Applied Mechanics, **55**, 831–836, doi: 10.1115/1.3173729.

Lumens, P., A. Franzen, K. Hornman, S. G. Karam, G. Hemink, B. Kuvshinov, J. La Follett, B. Wyker, and P. Zwartjes, 2013, Cable development for distributed geophysical sensing with a field trial in surface seismic: Fifth European Workshop on Optical Fibre Sensors, International Society for Optics and Photonics, 879435.

Lumens, P. G. E., 2014, Fibre-optic sensing for application in oil and gas wells: Ph.D. thesis, Technische Universiteit Eindhoven.

Madsen, K. N., M. Thompson, T. Parker, and D. Finfer, 2013, A VSP field trial using distributed acoustic sensing in a producing well in the north sea: First Break, **31**, 51–56.

Mateeva, A., J. Lopez, J. Mestayer, P. Wills, B. Cox, D. Kiyashchenko, Z. Yang, W. Berlang, R. Detomo, and S. Grandi, 2013, Distributed acoustic sensing for reservoir monitoring with VSP: The Leading Edge, **32**, 1278–1283, doi: 10.1190/tle32101278.1.

Mateeva, A., J. Mestayer, B. Cox, D. Kiyashchenko, P. Wills, J. Lopez, S. Grandi, K. Hornman, P. Lumens, A. Franzen, D. Hill, and J. Roy, 2012, Advances in distributed acoustic sensing (DAS) for VSP: 82nd Annual International Meeting, SEG, Expanded Abstracts, doi: 10.1190/segam2012-0739.1.

Mestayer, J., B. Cox, P. Wills, D. Kiyashchenko, J. Lopez, M. Costello, S. Bourne, G. Ugueto, R. Lupton, G. Solano, D. Hill, and A. Lewis, 2011, Field trials of distributed acoustic sensing for geophysical monitoring: 81st Annual International Meeting, SEG, Expanded Abstracts, 4253–4257.

Moore, J. P., and M. D. Rogge, 2012, Shape sensing using multi-core fiber optic cable and parametric curve solutions: Optics Express, **20**, 2967–2973, doi: 10.1364/OE.20.002967.

Stewart, R. R., J. E. Gaiser, R. J. Brown, and D. C. Lawton, 2003, Converted-wave seismic exploration: Applications: Geophysics, **68**, 40–57, doi: 10.1190/1.1543193.

Tsujikawa, K., K. Tajima, and J. Zhou, 2005, Intrinsic loss of optical fibers: Optical Fiber Technology, **11**, 319–331, doi: 10.1016/j.yofte.2005.04.003.

Uzunoglu, N. K., 1981, Scattering from inhomogeneities inside a fiber waveguide: JOSA, **71**, 259–273, doi: 10.1364/JOSA.71.000259.

Young, W. C., and R. G. Budynas, 2002, Roark's formulas for stress and strain: McGraw-Hill New York 7.

Downloaded 01/05/18 to 138.67.12.184. Redistribution subject to SEG license or copyright; see Terms of Use at http://library.seg.org/